Earthquake Geotechnical Engineering for Protection and Development of Environment and Constructions – Silvestri & Moraci (Eds)
© 2019 Associazione Geotecnica Italiana, Rome, Italy, ISBN 978-0-367-14328-2

Bridge-ground seismic response and liquefaction-induced deformations

Z. Qiu, A. Ebeido, A. Almutairi, J. Lu & A. Elgamal
Department of Structural Engineering, UC San Diego, La Jolla, USA

G. Martin
Department of Civil Engineering, USC, Los Angeles, USA

ABSTRACT: Global response of a bridge is dictated by soil-structure interaction considerations of the entire bridge-ground system. In order to capture the salient involved mechanisms, this study investigates numerically the longitudinal seismic performance of the entire bridge-ground system. For that purpose, two idealized three-dimensional finite element models are developed. As such, a realistic multi-layer soil profile is considered with interbedded liquefiable/non-liquefiable strata. Effect of the resulting liquefaction-induced ground deformation on the bridge-ground system is explored. Specific attention is drawn to the global deformation of the bridge structure as an integral entity due to lateral spreading effects in the vicinity of the abutments. The analysis techniques as well as the derived insights are of significance for general bridge-ground system configurations during liquefaction-induced ground deformation.

1 INTRODUCTION

Damage to large bridge overcrossings has been observed in recent earthquakes, including 2010 Maule (Arduino et al. 2010) and 2011 Christchurch (Cubrinovski et al. 2011, 2014). The observed response was often noted to be highly influenced by the global bridge-ground overall characteristics as an integral system. As such, investigators have been increasingly studying the entire bridge and the surrounding ground response within an integrated framework (Boulanger et al. 2007; Shin et al. 2007, 2008; Zhang et al. 2008; Ashford et al. 2009, 2011). Results of these studies show that consideration of the entire bridge-ground system provides a more realistic distribution of force and displacement demands. As such, it is indicated that global analysis is paramount in realistically evaluating the performance of liquefaction-induced lateral spreading and its consequences. On this basis, two representative three-dimensional (3D) finite element (FE) models were developed to investigate the consequences of liquefaction-induced ground deformation. In these two FE models, the actual pile-ground geometric configuration is captured.

2 COMPUTATIONAL FRAMEWORK

The Open System for Earthquake Engineering Simulation (OpenSees, McKenna et al. 2010) framework was employed to conduct nonlinear bridge-ground system analysis subjected to seismic excitations. Developed by the Pacific Earthquake Engineering Research (PEER) Center, OpenSees is widely used for simulation of geotechnical systems and soil-structure interaction applications (Yang & Elgamal 2002; Su et al. 2017). The OpenSees elements and materials used in this study are briefly described below.

Three-dimensional eight-node brick elements with two-phase material following the *u-p* formulation (Chan 1988) were employed for simulating saturated soil response, where u is the displacement of the soil skeleton and p is the pore water pressure. Calibrated in a large number of earlier studies, the employed soil constitutive models (Parra 1996; Yang 2000; Yang & Elgamal 2002; Elgamal et al. 2003) were PressureDependMultiYield03 and PressureIndependMultiyield (PIMY). Multi-yield surface incremental plasticity is used to generate nonlinear response with hysteresis damping, and to account for potential accumulated permanent deformations. The shear stress-strain backbone curve is represented by the hyperbolic relationship with the shear strength based on simple shear (reached at a octahedral shear strain of 10%). It is noted that PressureDependMultiYield03 (Khosravifar et al. 2018) includes new modifications to better capture the established guidelines on liquefaction triggering (Idriss & Boulanger 2008).

The FE matrix equation of the bridge-ground model is integrated in time using a single-step predictor multi-corrector scheme of the Newmark type (Chan 1988; Parra 1996) with integration parameters $\gamma = 0.6$ and $\beta = 0.3025$. The equation is solved using the modified Newton-Raphson method, i.e., Krylov subspace acceleration (Carlson & Miller 1998) for each time step. A relatively low level of stiffness proportional viscous damping was used to enhance numerical stability (coefficient = 0.003), with the main damping emanating from the soil nonlinear shear stress-strain hysteresis response (Su et al. 2017).

3 PILES AND SOIL-PILE INTERFACE

Three-dimensional nonlinear force-based beam-column elements with fiber-section (Scott & Fenves 2006; Scott & Ryan 2013) were employed to model the piles. Elastic beam-column elements (3D) were employed to simulate the deck, for simplicity. In order to represent the geometric space occupied by the pile in the soil domain, rigid beam-column links ($EI = 10^4$ times the linear EI of the pile) were used normal to the vertical axis of the pile (Elgamal et al. 2008). The 3D brick elements representing the soil were connected to the pile geometric configuration at the outer nodes of these rigid links (Law & Lam 2001) by using zerolength elements, zerolengthSection elements and the OpenSees equalDOF translation constraint (Elgamal et al. 2008). The zerolength and zerolengthSection elements are employed to axially connect the rigid links to adjacent soil node and provide skin friction yield shear force along the soil-pile interface according to the soil-pile friction angle and adhesion. As such, the skin friction is limited by $F = (c_A + \sigma' \tan\delta) \cdot l \cdot h / N$, where l is the perimeter of the pile, h is center to center contributing height (center of the pile to next pile center), c_A is the soil-pile adhesion, δ is the soil-pile friction angle, σ' is the lateral effective stress and N is the number of zeroLengthSection elements along the pile perimeter (Su et al. 2017).

4 NUMERICAL MODELING OF ENTIRE BRIDGE GROUND SYSTEM

4.1 *Ground configuration*

The overall ground configuration of Bridge 1 (Qiu 2020) is shown in Fig. 1a. In general, the site soil profile consists of shallow, fine-grained soils underlain by medium dense to dense sands, with loose sand layers (red zone Fig. 1a). A general summary of the characteristics for the subsurface soils is included in Table 1. The water table was taken at an elevation of 30.5 m as shown in Fig. 1a. The 18-span reinforced concrete bridge is approximately 197 m long and 9.9 m wide, and composed of a reinforced concrete deck on vertical pier walls with pile groups and on single piles. Two expansion joints (with a 0.05 m gap each, Fig. 1a) are located adjacent to the piers, respectively. In the longitudinal direction, a representative 1.83 m wide slice (Fig. 1a) was taken to represent the bridge's geometric configuration (Su et al. 2017).

The overall ground configuration of Bridge 2 (Qiu 2020) is shown in Fig. 1b. A general summary of the characteristics for the subsurface soils is included in Table 2. Of these soils, Layers Q2 and Q4 were deemed to be potentially liquefiable. Water table was measured to be approximately at elevation 28.8 m, located at the interface between Layers Q3a and Q3b. This 3-span reinforced concrete bridge is approximately 96 m long (spans of equal length) and 10.4 m wide, and composed of reinforced concrete pier walls, seat-type abutments and wing walls founded on steel H-piles. In the longitudinal direction, a representative 1.29 m wide slice (Fig. 1b) was taken to represent the bridge's geometric configuration (Su et al. 2017).

4.2 *FE models*

Based on the soil profiles shown in Tables 1 and 2 and ground configurations (Fig. 1), two idealized 3D bridge-ground FE models are developed (Fig. 2). The 3D FE models bear

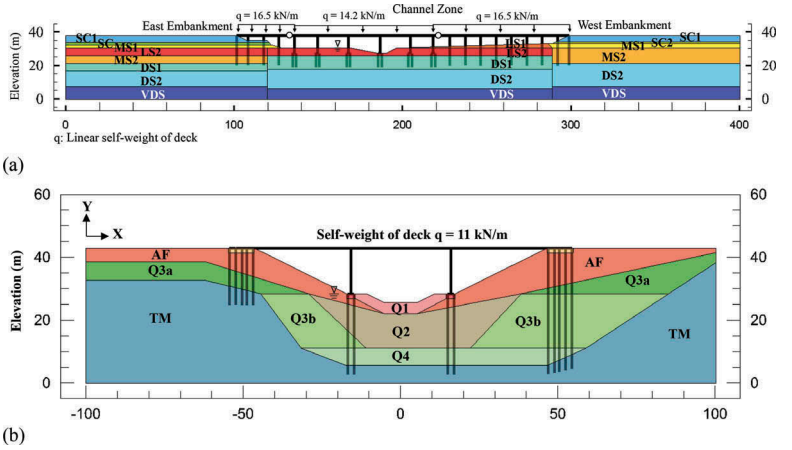

Figure 1. Ground configuration: (a) Bridge 1; (b) Bridge 2.

Table 1. Model parameters of Bridge 1*.

Soil unit	LS1/LS2	MS1/MS2	DS1	DS2	VDS	SC	SC1	SC2
Mass density (t/m^3)	1.98	2.03	2.08	2.08	2.13	2.07	2.1	2.1
Reference pressure (atm)	170	210	270	340	430	-	-	-
Low-strain shear modulus (MPa)	80.4	118	164	256	435	52.9	95.5	82.3
Friction angle	28°/29°	31°	34°	36°	40°	0	0	0
Cohesive strength (kPa)	2	2	2	2	2	24	96	48

* Qiu (2020) provides further details and full modeling parameters.

Table 2. Model parameters of Bridge 2*.

Soil unit	Q2	Q4	AF	Q1	Q3a	Q3b	TM
Mass density (t/m^3)	1.89	1.92	1.92	1.84	1.92	1.84	2.16
Reference pressure (atm)	2.0	2.7	-	-	-	-	-
Low-strain shear modulus (MPa)	73.8	103.4	117	71	139.3	75.2	293.0
Friction angle	35°	37°	0	0	0	0	0
Cohesive strength (kPa)	2	2	80	40	108	53	400

* Qiu (2020) provides further details and full modeling parameters.

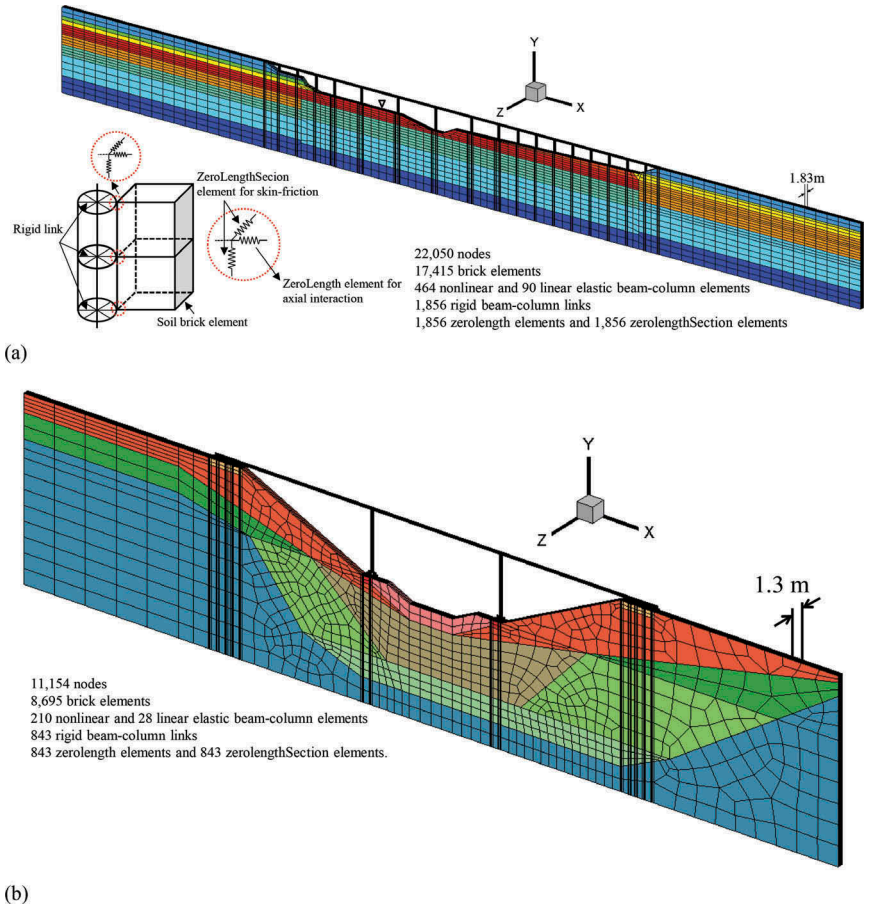

Figure 2. FE mesh: (a) Bridge 1; (b) Bridge 2.

similarity to the ubiquitous 2D plane-strain analysis approach. However, it naturally allows for a more precise representation of the actual 3D geometric pile layout and associated pile-soil interaction considerations. In this idealization, seismic response is investigated only in the longitudinal direction.

Along both side mesh boundaries (Fig. 2), 2D plane strain soil columns of large size and depth (not shown) are included (Su et al. 2017). These soil columns, at an adequate distance away from the bridge structure to minimize boundary effects (Fig. 2), efficiently reproduce the desired free-field site response at these locations.

4.3 *Boundary and loading conditions*

As mentioned above, both lateral boundaries are located relatively far away from the bridge structure (Fig. 2). Along the soil longitudinal symmetry planes, no out of plane motion is allowed. The loading conditions were implemented in a staged fashion as follows:

1. Gravity was applied to activate the initial static state for the soil domain only with: i) linear elastic properties (Poisson's ratio of 0.47 for all layers), ii) nodes on both side planes of the model fixed against longitudinal translation, iii) nodes along the base fixed against vertical translation, iv) water table prescribed (Fig. 2) with related water pressure and nodal forces specified along the canyon boundary. At the end of this step, the static soil state was

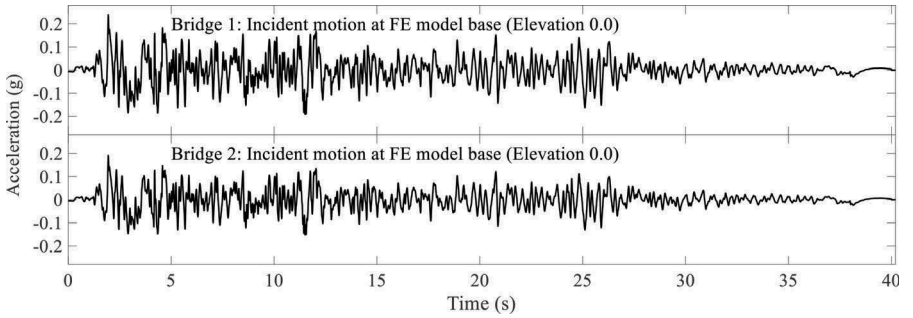

Figure 3. Input motions.

imposed and displacements under own-weight application were re-set to zero using the OpenSees command InitialStateAnalysis.
2. Soil properties were switched from linear elastic to plastic (Tables 1 and 2)
3. Nonlinear force-based beam-column elements of pile and elastic beam-column elements of reinforced concrete deck were added. The pile nodes were connected to the soil nodes by rigid links, zerolength and zerolengthSection elements as described above. Thereafter, self-weight of the bridge structure was applied.

In this study, the Lysmer-Kuhlemeyer 1969 boundary is applied along the base of the FE model (base V_s = 600 m/s, slightly higher than the stiffness of the overlying stratum), so as to avoid spurious wave reflections along this model boundary. For the shaking phase (purely in the longitudinal x-direction), seismic motion was simply taken as that of the 1940 Imperial Valley earthquake ground surface El Centro Station record, scaled down to a peak amplitude of about 0.4 g. Via deconvolution (using Shake91, Idriss & Sun 1993), an incident earthquake motion (Fig. 3) was derived and imparted (Elgamal et al. 2008) along the base of the FE model (elevation 0.0 in Fig. 1). In this representation, free-field site response along both the side mesh boundaries is generated by the included 2D plane strain soil columns mentioned above.

5 DEFORMATION

Fig. 4 displays the lateral displacement of the bridge deck with a permanent displacement of 0.15 m and -0.1 m, respectively, indicating two different overall deformation patterns. As such, the deformed mesh at end of shaking will be discussed and the permanent deformation patterns of the two entire bridge-ground systems will be investigated.

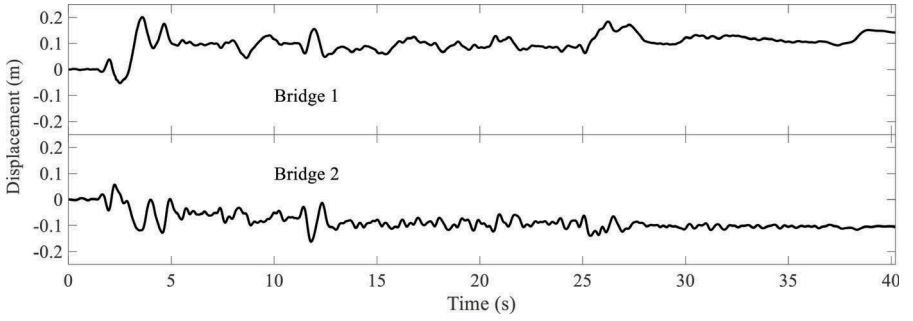

Figure 4. Deck displacement.

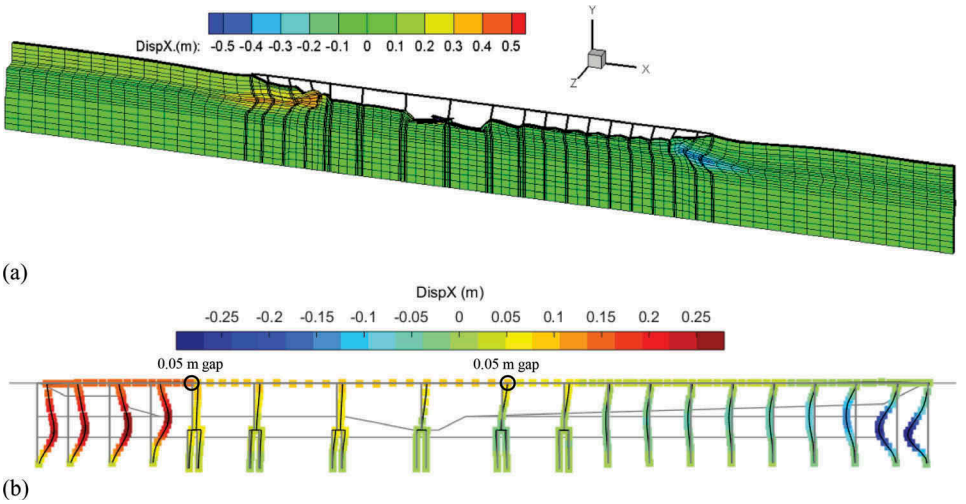

Figure 5. Deformed mesh (factor of 15): (a) Bridge-ground system; (b) Structure.

5.1 *Bridge 1*

Fig. 5a depicts the deformed mesh of Bridge 1 at end of shaking (colors show horizontal displacement). Away from the bridge, lateral deformation above the liquefied strata was to the right, about 0.2 m on the left-side and only 0.008 m on the right-side. Superposed on this global displacement pattern (to the right), local downslope deformations are seen on both sides of the bridge (Fig. 5a). Near the abutments, additional downslope deformation relative to the surrounding ground was about 0.35 m (left-side), and 0.4 m (right-side). Due to the downslope deformations at both sides, the bridge deck through its piers and foundations acts as a strut that provides added restraint to the slope deformations on both sides.

Fig. 5b displays lateral displacement of the bridge structure at end of shaking with a peak displacement of about 0.27 m on both sides. As discussed above, both east and west embankments moved downslope into the channel zone, such that the entire bridge deck was in a compressive state and appreciable deck axial force was attained (not shown).

5.2 *Bridge 2*

Fig. 6a depicts the deformed mesh of Bridge 2 at end of shaking (colors show horizontal displacement). The local downslope deformation on both slopes reached about 0.65 m and 0.2 m, respectively. For this particular relatively narrow canyon geometry (Fig. 1), an interference deformation pattern (Fig. 6a) was observed due to the local downslope deformations on both slopes. As a result, soil in central sections experienced a tendency for moving upward (Fig. 6a). It is noted that the lateral deformation on both side boundaries away from the bridge was small (about 0.04 m in Fig. 6a). As such, the global displacement was mainly dominated by local downslope deformations on both slopes.

Fig. 6b shows lateral displacement of bridge structure at end of shaking with a peak displacement of about 0.6 m. Both slopes moved downslope into the center of narrow canyon, such that the entire bridge deck was in a compressive state and appreciable deck axial force was attained (not shown).

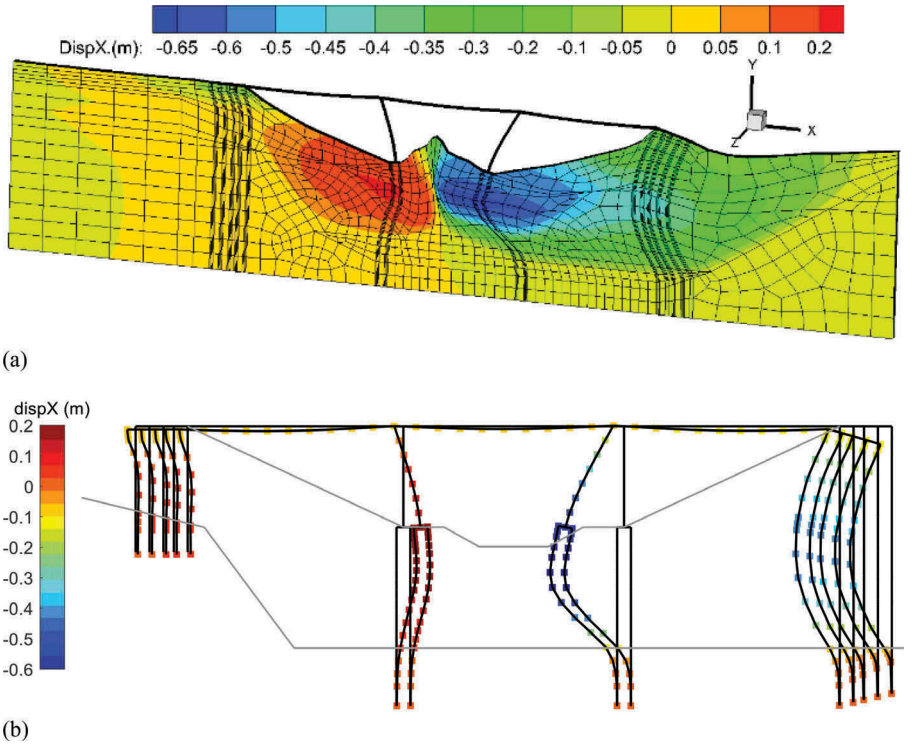

Figure 6. Deformed mesh (factor of 15): (a) Bridge-ground system; (b) Structure.

6 SUMMARY AND CONCLUSIONS

A 3D FE analysis framework was presented to study the liquefaction-induced seismic response of bridge-ground systems dictated by soil-structure interaction. For that purpose, two idealized OpenSees 3D FE models with different geometric ground configurations were developed. The bridge-ground systems and the corresponding numerical analysis details were discussed. Permanent deformation patterns resulting from the liquefaction-induced lateral spreading were explored. The numerical framework and the insights derived from this study are of general relevance to bridge-ground seismic response scenarios.

Specific observations and conclusions include: 1) As highlighted in earlier studies (Shin et al. 2007, 2008; Zhang et al. 2008), response is highly dependent on the soil ground system as an integral global entity. Connectivity provided by the bridge deck, soil profile and its variation along the bridge length, and geometric configuration of the slopes and the underlying water channel are all factors that can significantly influence the outcome. 2) Local slope deformations occur along with additional overall permanent ground lateral deformation (due to asymmetry of the input ground motion and its response characteristics), which might contribute to higher demands due to the combined result of both.

ACKNOWLEDGEMENTS

This research was supported by the California Department of Transportation (Caltrans) under Contract No. 65A0548 with Dr. Charles Sikorsky as the project manager. This support is most appreciated. In addition, we are grateful for the valuable technical suggestions, comments and contributions provided by Mr. Fadel Alameddine of Caltrans.

REFERENCES

Arduino, P., Ashford, S., Assimaki, D., Bray, J., Eldridge, T., Frost, D., Hashash, Y., Hutchinson, T., Johnson, L., Kelson, K. & Kayen, R. 2010. *Geo-engineering reconnaissance of the 2010 Maule, Chile earthquake*. GEER Association Report No. GEER-022, 1.

Ashford, S.A., Boulanger, R.W., Brandenberg, S.J. & Shantz, T. 2009. Overview of Recommended Analysis Procedures for Pile Foundations in Laterally Spreading Ground. In TCLEE 2009: *Lifeline Earthquake Engineering in a Multihazard Environment*, 1–8.

Ashford, S.A., Boulanger, R.W. & Brandenberg, S.J. 2011. Recommended design practice for pile foundations in laterally spreading ground. *Pacific Earthquake Engineering Research Center. University of California, Berkeley, Calif*. PEER Rep, (2011/04).

Boulanger, R.W., Chang, D., Brandenberg, S.J., Armstrong, R.J. & Kutter, B.L. 2007. Seismic design of pile foundations for liquefaction effects. In *Earthquake Geotechnical Engineering*, 277–302. Springer, Dordrecht.

Carlson, N.N. & Miller, K. 1998. Design and application of a gradient-weighted moving finite element code I: in one dimension. *SIAM Journal on Scientific Computing*, 19(3): 728–765.

Chan, A.H.C. 1988. A unified finite element solution to static and dynamic problems in geomechanics. PhD Thesis, University College of Swansea.

Cubrinovski, M., Bradley, B., Wotherspoon, L., Green, R., Bray, J., Wood, C., Pender, M., Allen, J., Bradshaw, A., Rix, G. & Taylor, M. 2011. Geotechnical aspects of the 22 February 2011 Christchurch earthquake.

Cubrinovski, M., Winkley, A., Haskell, J., Palermo, A., Wotherspoon, L., Robinson, K., Bradley, B., Brabhaharan, P. & Hughes, M. 2014. Spreading-induced damage to short-span bridges in Christchurch, New Zealand. *Earthquake Spectra*, 30(1): 57–83.

Elgamal, A., Yang, Z. & Parra, E. 2003. Modeling of cyclic mobility in saturated cohesionless soils. *International Journal of Plasticity*, 19(6): 883–905.

Elgamal, A., Yan, L. & Yang, Z. 2008. Three-dimensional seismic response of Humboldt Bay bridge-foundation-ground system. *Journal of Structural Engineering*, 134(7): 1165–1176.

Idriss, I.M. & Sun, J.I. 1993. User's manual for SHAKE91: A computer program for conducting equivalent linear seismic response analyses of horizontally layered soil deposits. *Center for Geotechnical Modeling, Dept. of Civil and Environmental Engineering, University of California Press*, *Davis, CA*.

Idriss, I. M. & Boulanger, R. W. 2008. Soil liquefaction during earthquakes. *Earthquake Engineering Research Institute*.

Khosravifar, A., Elgamal, A., Lu, J. & Li, J. 2018. A 3D model for earthquake-induced liquefaction triggering and post-liquefaction response. *Soil Dynamics and Earthquake Engineering*, 110: 43–52.

Lysmer, J. & Kuhlemeyer, R.L. 1969. Finite Dynamic Model for Infinite Media. *Journal of Engineering Mechanics Division*, 95: 859–878.

McKenna, F., Scott, M.H. & Fenves, G.L. 2010. Nonlinear finite-element analysis software architecture using object composition. *Journal of Computing in Civil Engineering*, 24(1): 95–107.

Parra, E. 1996. Numerical modeling of liquefaction and lateral ground deformation including cyclic mobility and dilation response in soil systems. PhD Thesis. Rensselaer Polytechnic Institute.

Qiu, Z. 2020. Constitutive modeling and numerical simulation of soil-structure interaction due to liquefaction. PhD Thesis, Dept. of Structural Engineering, University of California, San Diego, La Jolla, CA.

Scott, M.H. & Fenves. G.L. 2006. Plastic hinge integration methods for force-based beam-column elements. *Journal of Structural Engineering*, 132(2): 244–252.

Scott, M.H. & Ryan, K.L. 2013. Moment-rotation behavior of force-based plastic hinge elements. *Earthquake Spectra*, 29(2): 597–607.

Shin, H., Arduino, P. & Kramer, S.L. 2007. Performance-based evaluation of bridges on liquefiable soils. In *Structural Engineering Research Frontiers*: 1–16.

Shin, H., Arduino, P., Kramer, S.L. & Mackie, K. 2008. Seismic response of a typical highway bridge in liquefiable soil. In *Geotechnical Earthquake Engineering and Soil Dynamics IV*, 1–11.

Su, L., Lu, J., Elgamal, A. & Arulmoli, A.K. 2017. Seismic performance of a pile-supported wharf: Three-dimensional finite element simulation. *Soil Dynamics and Earthquake Engineering*, 95: 167–179.

Yang, Z. 2000. Numerical modeling of earthquake site response including dilation and liquefaction. PhD Thesis, Columbia University.

Yang, Z. & Elgamal, A. 2002. Influence of permeability on liquefaction-induced shear deformation. *Journal of Engineering Mechanics*, 128(7): 720–729.

Zhang, Y., Conte, J.P., Yang, Z., Elgamal, A., Bielak, J. & Acero, G. 2008. Two-dimensional nonlinear earthquake response analysis of a bridge-foundation-ground system. *Earthquake Spectra*, 24(2): 343–386.